ACS APPLIED MATERIALS & INTERFACES

Research Article

www.acsami.org

Enhanced Electrochemical Performance with Surface Coating by Reactive Magnetron Sputtering on Lithium-Rich Layered Oxide Electrodes

Bao Qiu,[†] Jun Wang,[‡] Yonggao Xia,*[,†] Zhen Wei,[†] Shaojie Han,[†] and Zhaoping Liu*[,†]

[†]Ningbo Institute of Materials Technology and Engineering (NIMTE), Chinese Academy of Sciences, Ningbo, Zhejiang 315201, China

[‡]MEET Battery Research Center/Institute of Physical Chemistry, University of Muenster, Corrensstrasse 46, 48149 Muenster, Germany

ABSTRACT: Electrode films fabricated with lithium-rich layered $0.3Li_2MnO_3-0.7LiNi_{5/21}Co_{5/21}Mn_{11/21}O_2$ cathode materials have been successfully modified with ZnO coatings via a reactive magnetron sputtering (RMS) process for the first time. The morphology and chemical composition of coating films on the electrodes have been in deep investigated by transmission electron microscopy (TEM), energy dispersive spectrometry (EDS), and X-ray photoelectron spectroscopy (XPS) characterizations. The results clearly demonstrate that ZnO film coatings are ultrathin, dense, uniform, and fully covered on the electrodes. The RMS-2 min (deposition time) coated electrode exhibits much higher initial discharge capacity and coulombic efficiency with 316.0 mAh g^{-1} and 89.1% than that of the pristine electrode with 283.4 mAh g^{-1} and 81.7%. In addition, the discharge capacity also reaches 256.7 and 187.5 mAh g^{-1} at 0.1 and 1.0 C-rate, as compared to that of 238.4 and 157.8 mAh g^{-1} after 50 cycles. The improved electrochemical performances of RMS-coated electrodes are ascribed to the high-quality ZnO film coatings that reduce charge transfer resistance and effectively protect active material from electrolyte oxidation.

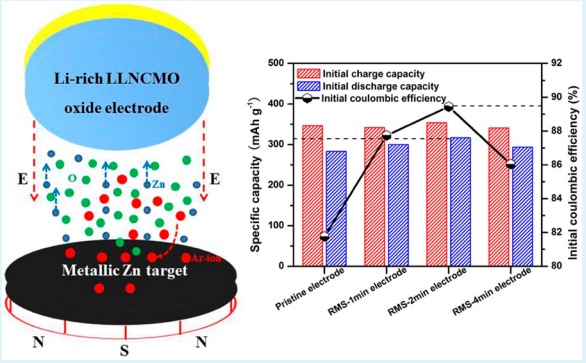

KEYWORDS: *lithium-ion batteries, lithium-rich layered oxide cathode, zinc oxide coating, reactive magnetron sputtering, initial coulombic efficiency*

1. INTRODUCTION

Rechargeable lithium-ion batteries (LIBs) are being considered as the key technology of choice for powering electric vehicles (EVs) due to their long service life and high energy density.[1,2] However, it is clear for EVs that the energy density of LIBs must be exceeding 250 Wh kg^{-1}.[3] To this end, it is necessary to focus on greater capacity cathode materials to substitute for the currently used $LiCoO_2$, $LiMn_{1/3}Ni_{1/3}Co_{1/3}O_2$, and $LiNi_{0.85}Co_{0.1}Al_{0.05}O_2$, of which these cathode materials only deliver the capacity of less 200 mAh g^{-1}.[4−6] A new layered oxide possessing excess Li in the transition metal layer, denoted either as $xLi_2MnO_3-(1-x)LiMO_2$ (M = Mn, Ni, and Co) or $Li[Li_{1/3-2x/3}Ni_xMn_{2/3-x/3}]O_2$, was recently reported.[7,8] Such a finding has received worldwide attention, owing to its discharge capacity of over 250 mAh g^{-1}, low cost and high safety.[9−11]

Unfortunately, they also suffer from some disadvantages with initially large capacity loss and poor rate capacity.[12−17] This is generally caused by the initial charge process, which is typically different from that of the currently used layered materials.[4] As reported in previous literatures, this process can be divided into two stages.[8,12,18] When the charge voltage vs Li^+/Li is below 4.4 V, lithium ions can be extracted from the $LiMO_2$ component. After charged to over 4.4 V, a long plateau would form at 4.5 V, which is accompanied by extracting a net loss of Li_2O from the Li_2MnO_3 component.[19] The net loss of Li_2O leads to a huge irreversible capacity loss in the initial cycle.[8,19] Meanwhile, some oxygen extracted from the lattice results in the transition metal ions migration leading to phase transformation, especially on the surface of the materials.[19,20] This irreversible phase transformation is adverse to high rate capability as demonstrated by Xu et al.[20] In order to further improve the electrochemical performance, many approaches including surface modification,[21,22] blend in lithium-intercalated hosts,[23] and special nanostructures[24] on these high-capacity materials have been developed. Among these strategies, more effective approach to lower or eliminate the initially irreversible capacity is surface modification, such as oxide,[21,22,25] fluoride,[26] and phosphate.[27] Nonetheless, most surface modifications of lithium-rich layered oxides reported in literatures are carried out with wet chemical method such as sol−gel or solution

Received: March 4, 2014
Accepted: May 23, 2014
Published: May 23, 2014

processing with soaking cathode materials into a metal-ions-contained sol.[21,22,26,27] These processes are not well-controlled. As a consequence, it is apparent that the lack of control over thickness and uniformity is prohibited by sol-gel methods. Therefore, it is significant to explore new surface coatings that are much thinner and have high uniformity for next generation battery technology.

So far, many techniques preparing surface coating films have been brought in the battery technology, such as atomic layer deposition (ALD),[28−30] thermal evaporation (TE),[31,32] and pulsed laser deposition (PLD).[33] Among these techniques, ALD has been extensively applied in lithium-rich Li-$[Li_{0.2}Mn_{0.54}Ni_{0.13}Co_{0.13}]O_2$,[28] nano-sized $LiCoO_2$,[29] and spinel $LiMn_2O_4$.[30] It significantly enhances their electrochemical performances after ALD coatings, but the alkyl-metal salts used as precursors to form ALD coatings are apparently restricted its large-scale application; at the same time, another technique about reactive magnetron sputtering (RMS) plays an important role in preparing coating film for photoluminescence and thermoelectric material.[34,35] It has several advantages:[36] (1) low substrate temperature (down to room temperature); (2) good adhesion of films on substrate materials; (3) very good thickness uniformity; and (4) directive deposition from elemental (metallic) targets by reactive sputtering in rare/reactive gas mixtures. In addition, the deposition process can be easily repeated. There are some reports about surface modifications of LIBs electrode via radio-frequency magnetron sputtering coatings at spinel $LiMn_2O_4$ cathode.[37,38] Therefore, we believe RMS coating may be an attractive method to improve the electrochemical performance in lithium-rich layered oxides.

Anther factor to consider is to choose appropriate surface coatings. The semiconducting ZnO film has been successfully applied in lithium-rich layered oxide to improve their electrochemical performance.[39,40] For instance, Wu et al.[39] successfully constructed ZnO-layer coating with Li-$[Li_{0.2}Ni_{0.13}Co_{0.13}Mn_{0.54}]O_2$, leading to the result that the irreversible capacity loss was significantly reduced. Recently, Singh et al.[40] reported that the $Li[Li_{0.2}Ni_{0.2}Mn_{0.6}]O_2$ electrode coated with ZnO exhibited enhanced cycle life. In the present paper, lithium-rich $0.3Li_2MnO_3-0.7LiNi_{5/21}Co_{5/21}Mn_{11/21}O_2$ oxides were synthesized by a co-precipitation method, and RMS process with ZnO film coatings is firstly introduced in directly coating on the $0.3Li_2MnO_3-0.7LiNi_{5/21}Co_{5/21}Mn_{11/21}O_2$ electrodes as shown in Figure 1. In here, we prepared ZnO film by RMS using a metallic Zn target. Ionized Ar ions were generated in glow discharge plasma and then accelerated by an electric field to bombard the target. This bombardment caused the removal of metallic Zn target atoms, in which reacted with oxygen to generate zinc oxide and finally condensed onto the substrate electrode as a thin film. It is expected that the discharge capacity, rate capacity, and cycle stability would be greatly improved by RMS coatings on the electrodes.

2. EXPERIMENTAL SECTION

2.1. Synthesis of Lithium-Rich $0.3Li_2MnO_3$-$0.7LiNi_{5/21}Co_{5/21}Mn_{11/21}O_2$ (LMO-NCM) Oxides. Lithium-rich layered oxide with a nominal formula $0.3Li_2MnO_3-0.7LiNi_{5/21}Co_{5/21}Mn_{11/21}O_2$ was synthesized through solid-state reaction between Li_2CO_3 and $(Ni_{1/4}Co_{1/4}Mn_{4/6})CO_3$ powders. The mole ratio between them was set to 0.65. The mixed precursor was firstly pre-treated at 500 °C for 5 h and then calcined at 850 °C for 15 h. The $(Ni_{1/4}Co_{1/4}Mn_{4/6})CO_3$ precursor was prepared as follows: an aqueous solution containing $NiSO_4·6H_2O$, $CoSO_4·7H_2O$, and $MnSO_4·5H_2O$ with a concentration of 2.0 mol L^{-1} was pumped into a stirring tank reactor; and then 2 M Na_2CO_3 solution and 0.2 M NH_4OH solution were separately added into the reactor. The temperature was held at 60 °C, and the pH value was fixed to 8.0. The resulting powders were washed several times by pure water to remove Na^+, and dried in a vacuum oven at 100 °C for more than 20 h.

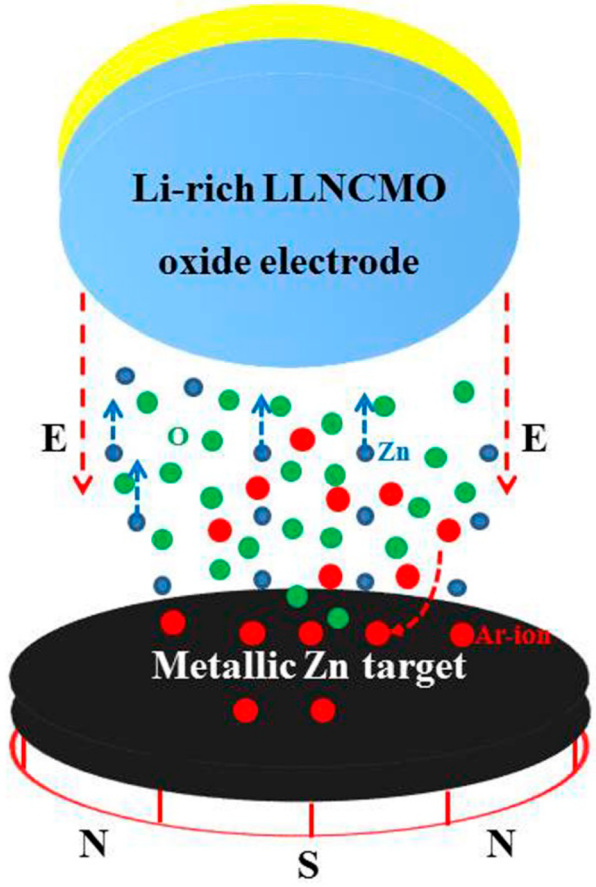

Figure 1. Schematic diagram showing reactive magnetron sputtering process for ZnO film deposition on the lithium-rich LLNCMO oxide electrode.

2.2. Surface Coatings by Reactive Magnetron Sputtering on Lithium-Rich Layered Oxide Electrodes. The bare composite electrode (abbreviated as pristine electrode) was prepared by spreading a mixture of the LMO-NCM powder (80 wt %), acetylene black (10 wt %), and polyvinylidenefluoride as the binder (10 wt %) dissolved in *N*-methyl pyrrolidone (NMP). The slurry was coated onto the aluminum current collector with the thickness setting of 350 μm and dried overnight at 120 °C in a vacuum oven. Approximately 7 mg of active material was loaded in the circular working electrode with a diameter of 14 mm.

Surface coatings of the electrode film with ZnO film are conducted by reactive magnetron sputtering (RMS) on carbon/aluminum foil substrates using a metallic Zn target (99.99%). High purity argon and oxygen were used as the sputtering and reactive gas, respectively. The target-to-substrate distance was 10 cm. The cathode was mounted on a water-cooled copper plate. The chamber was pumped to a base pressure of 1×10^{-4} Pa before deposition. Film growth was carried out in the growth ambient with a mixture of argon (40%) and oxygen (60%), and at a constant working pressure of 0.30 Pa. The film thickness was carried out by strictly controlling the deposited time. In here, the deposited time on the electrode was set at 1, 2, and 4 min, respectively (abbreviated as RMS-1 min, RMS-2 min, and RMS-4 min electrode).

2.3. Characterizations. Different composite electrodes were performed by X-ray diffraction (XRD) on a German Bruker D8 Advanced X-ray Diffractometer with Cu Kα radiation at a voltage of 40 kV and a current of 40 mA. Field emission scanning electron microscopy (FESEM) images were acquired on a FEI Quanta 250 FEG microscope, equipped with elemental mapping. The surface coating was observed by an FEI Tecnai G2 F20 transmission-electron microscope (TEM) at an accelerating voltage of 200 kV equipped with energy dispersive spectrometry (EDS). The detailed procedure is as follows: sample powder was firstly scraped off the RMS-4 min electrode and then dispersed in NMP solution, and the mixed solution was dropped onto thick amorphous carbon films supported on the copper grids. X-ray photoelectron spectroscopy (XPS) measurements were conducted using an AXIS Ultra DLD spectrometer with Al Kα (1253.6 eV) radiation. The as-obtained electrodes after MRS coatings were directly used to detect the change of surface compositions. The base pressure in the XPS analysis was 3×10^{-10} Torr. During the data acquisition, the constant analyzer energy mode was employed at a step size between 0.25 and 0.50 eV. To further collect the electrodes after initially charged to 4.5 and 4.8 V, coin-type cells were disassembled in an argon-filled glove box, washed with anhydrous dimethyl carbonate (DMC), and dried under vacuum overnight. The as-obtained electrodes were used for further XPS analyses to determine the changes of the compositions on the electrode surface. Curve fitting of slow-scanned XPS spectra was carried out using a peak-fit program with a Gaussian−Lorentzian sum function. The C 1s peak (284.6 eV) from the adventitious carbon was used as the reference for binding energy calibration.

2.4. Electrochemical Measurements. Different composite electrodes were assembled into CR2032-type coin cells for electrochemical tests, with lithium-rich composite electrode as cathode, metallic lithium foil as anode, and Celgard-2502 membrane as separator in an argon-filled glovebox; the electrolyte was 1 M $LiPF_6$ dissolved in ethylene carbonate (EC) and dimethyl carbonate (DMC) at a volumetric ratio of 3:7. The cells were galvanostatically charged and discharged on a LAND-CT2001A battery test system. Unless otherwise specified, the cells were typically cycled between 2.0 to 4.8 V vs Li^+/Li^0, and 1.0 C-rate was equal to the current density of 250 mA g^{-1}. Electrochemical impedance spectroscopy (EIS) measurements were conducted by Autolab83710 impedance analyzer with an amplitude voltage of 5 mV and frequency range of 0.0−100 000 Hz. Before EIS measurements, all cells were initially charged to 4.5 and 4.8 V at 0.1 C-rate. Li foil served as both counter and reference electrodes during the EIS measurements. All the electrochemical measurements were conducted at room temperature.

3. RESULTS AND DISCUSSION

3.1. Characterizations of the Surface Coatings on the Electrodes. Figure 2 compares the XRD patterns of the pristine and MRS-coated lithium-rich LMO-NCM electrodes. The major peaks of the XRD pattern for the pristine electrode (Figure 2a) are well indexed to α-$NaFeO_2$ hexagonal type structure for $LiCoO_2$ with space group symmetry of $R\bar{3}m$.[41,42] Some of the high intensity peaks corresponding to the Al are contributed to the Al-foil onto which the cathode material has been coated. The low intensity peaks in 2θ between 20° and 30° show the presence of monoclinic Li_2MnO_3 component with space group symmetry of $C2/m$.[41,42] This indicates the formation of the well crystalline layered structure. Compared to the pristine electrode, the XRD patterns for RMS-coated electrodes (Figure 2b−d) have no clear changes. The absence of any reflections corresponding to the Zn-contained product in the RMS-coated electrodes is possibly due to its amorphous nature or low concentration.

To confirm the formation of Zn-contained product on the electrode surface, parts a and b of Figure 3 show the FESEM images and related-element mappings of the pristine electrode

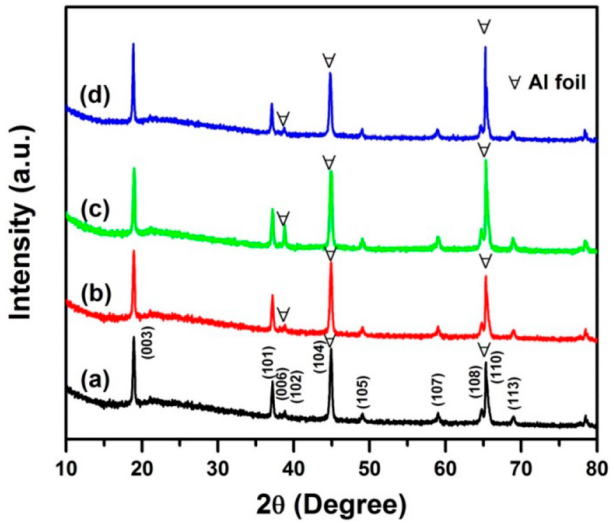

Figure 2. XRD patterns of different electrodes: (a) pristine electrode, (b) RMS-1 min electrode, (c) RMS-2 min electrode, and (d) RMS-4 min electrode.

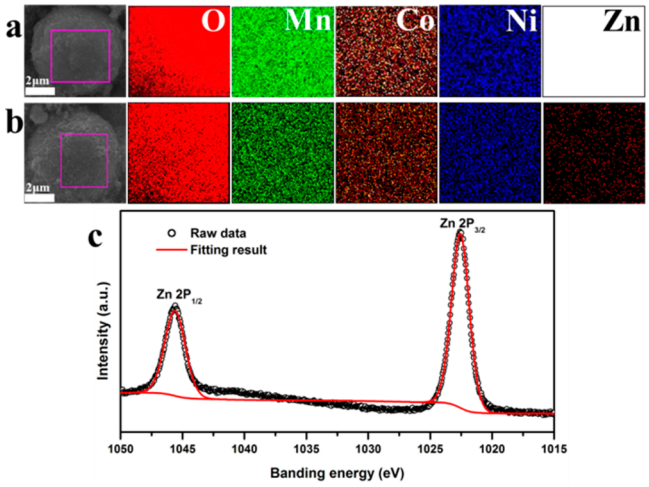

Figure 3. (a, b) SEM image and elemental mappings of the pristine electrode and the RMS-4 min electrode, respectively; (b) the XPS spectrum of Zn 2p of the RMS-4 min electrode.

and the RMS-4 min coated LMO-NCM on the electrode, respectively. It is observed that the as-obtained powder sample is spherical particles. More importantly, the dot mapping clearly reveals that element Zn is uniformly distributed on the surface of the RMS-4 min electrode, compared to that of the pristine electrode without detecting the existence of Zn element. Additionally, XPS is a sensitive tool for the surface composition, especially for the change of chemical state, and therefore used to determine the presence of Zn-contained product on the surface. The Zn 2p XPS spectrum for the RMS-4 min electrode is shown in Figure 3b. Presence of the Zn on the surface electrode is also reflected by the presence of the sharp peaks corresponding to Zn 2p peaks. It is worth noting that the observed binding energy of the Zn $2p_{3/2}$ remains to be 1022.6 eV, which is larger than the value of Zn $2p_{3/2}$ in bulk ZnO (The standard value about 1021.7 in NIST XPS Database) and metallic Zn with a binding energy of 1021.5 eV.[43] The value is very close to the reported values of ZnO-coated cathode materials, for example, 1022.5 eV for ZnO-coated Li-

dx.doi.org/10.1021/am501293y | ACS Appl. Mater. Interfaces 2014, 6, 9185−9193

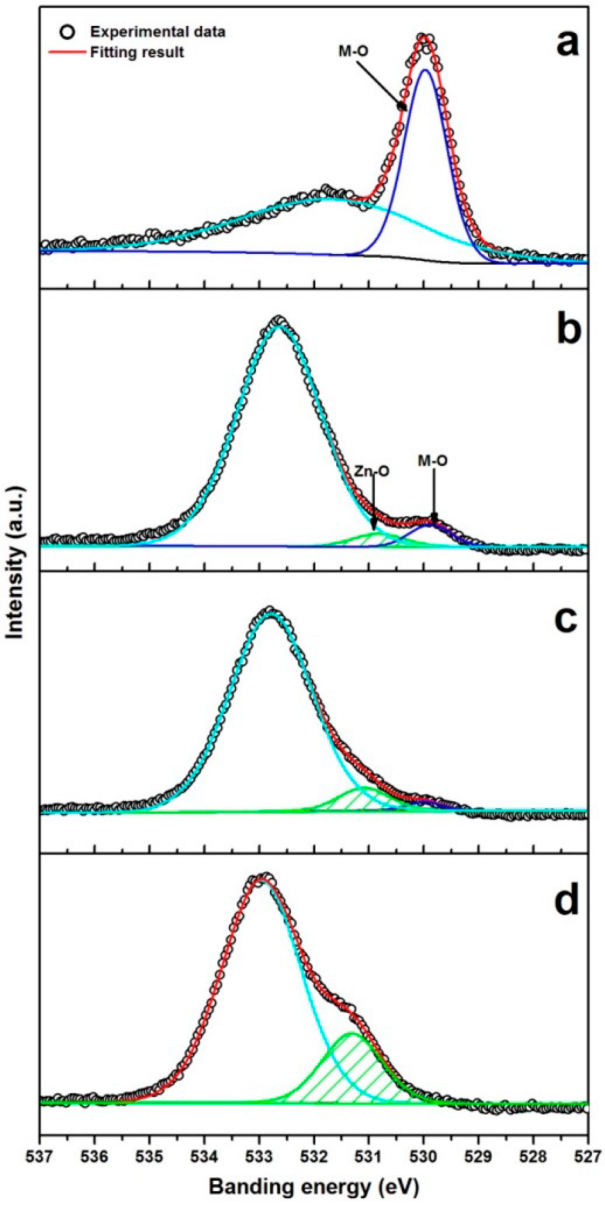

Figure 4. XPS spectra of the O 1s with different electrodes: (a) pristine electrode, (b) RMS-1 min electrode, (c) RMS-2 min electrode, and (d) RMS-4 min electrode.

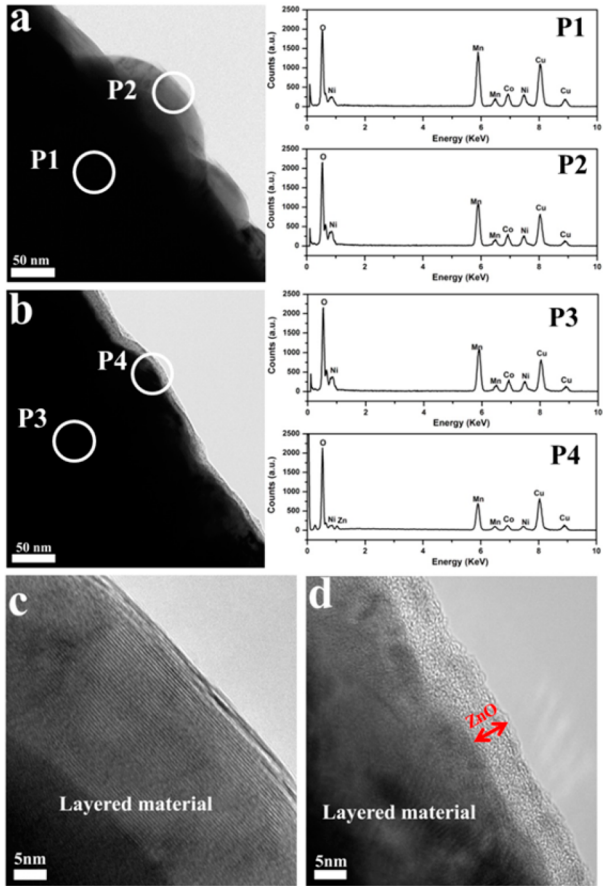

Figure 5. (a, b) TEM image of the pristine electrode and RMS-4 min electrode. The EDS signals of the areas labeled as p1, p2 and p3, p4 are shown in the right, respectively. HRTEM images of the particle on the (c) pristine electrode and (d) RMS-4 min electrode.

$Ni_{0.5}Co_{0.25}Mn_{0.25}O_2$[44] and 1022.2 eV for ZnO-coated Li-$Ni_{0.5}Mn_{1.5}O_4$.[45] This shows that Zn exists only in the oxidized state and is mainly bivalent. Therefore, it is concluded that the ZnO film as expected has successfully formed on the composite electrode.

Surface characteristic even for oxygen species is one of the contributing factors to affect the electrochemical performance.[46] Figure 4a shows the O 1s XPS spectra of the pristine electrode. It is clear that the asymmetric O 1s peak was coherently fitted by two completely Gaussian components and is located at 531.7 and 529.9 eV. The former is possibly correlated to OH^- or adsorbed H_2O environment,[47] the latter clearly contributed to the lattice of oxygen in the lithium-rich layered oxide.[48] While the electrodes after RMS coatings show large changes, as given in Figure 4b–d, the asymmetric O 1s peak on the electrode was fitted by three nearly Gaussian components, approximately centered at 529.9, 531.4, and 532.8 eV, respectively. The lower banding energy is the same as the value of the pristine electrode ascribed to the M–O covalence.[48] The higher binding energy is usually attributed to adsorbed or dissociated oxygen, or $-CO_3$ that may be originated from the oxidation of C-contained compounds.[46,47] The medium banding energy in the RMS coated electrode may be associated with O^{2-} ions within the ZnO matrix. However, the value is much larger than that of the O^{2-} ions (530.2 eV) on the regular wurtzite structure of the hexagonal Zn^{2+} ion array.[49] The same phenomenon has been also observed by Kunat et al.[50] They contributed it to oxygen-deficient regions within the ZnO matrix. Recently, Kotsis et al.[51] calculated the O 1s core level binding energies in different Zn-contained compounds by means of wave function based quantum chemical ab initio methods, and the result was in excellent agreement with the experimental data. Therefore, we believe the medium banding energy is resulted from ZnO film with some oxygen defects. More interestingly, the intensity about this peak gradually increases with the deposited time increasing. By contrast, the intensity about the lower banding energy peak gradually decreases with the thickness of ZnO film increasing. This is caused by the depth of penetration for X-ray. After the calculation, the intensity of the medium banding energy peak for the RMS-4 min electrode is about 2.5 times for that of the RMS-2 min electrode which is approximately 2.5 times for that of the RMS-1 min electrode. This further indicates that ZnO

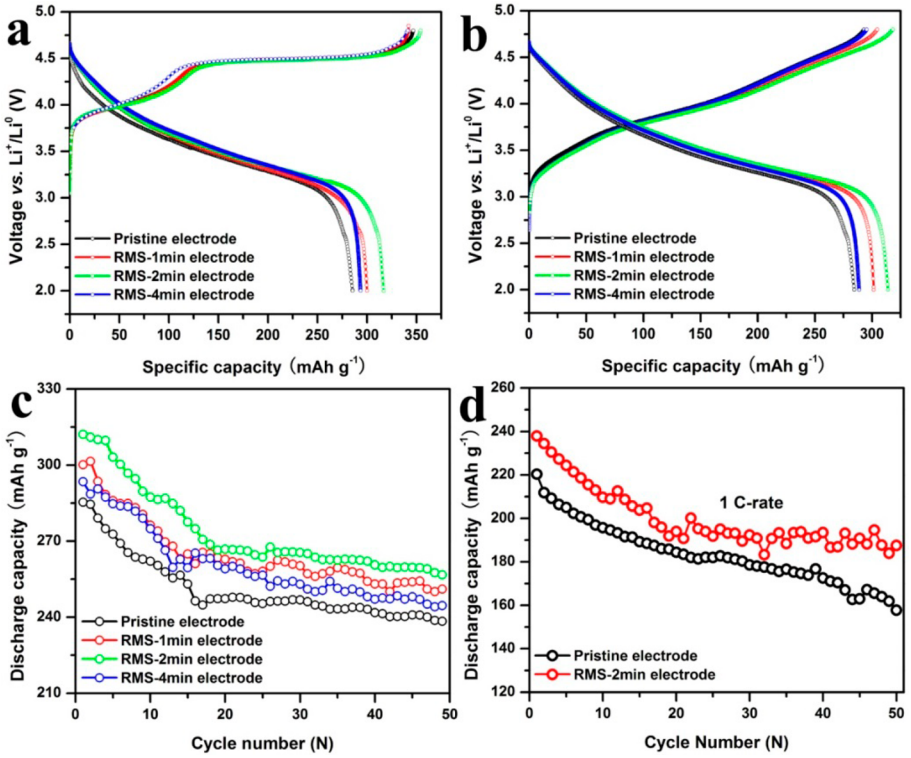

Figure 6. Typical charge−discharge curves for different electrodes: (a) the first cycle and (b) the second cycle. Cycling performances at different rates for different electrodes: (c) 0.1 C-rate and (d) 1.0 C-rate.

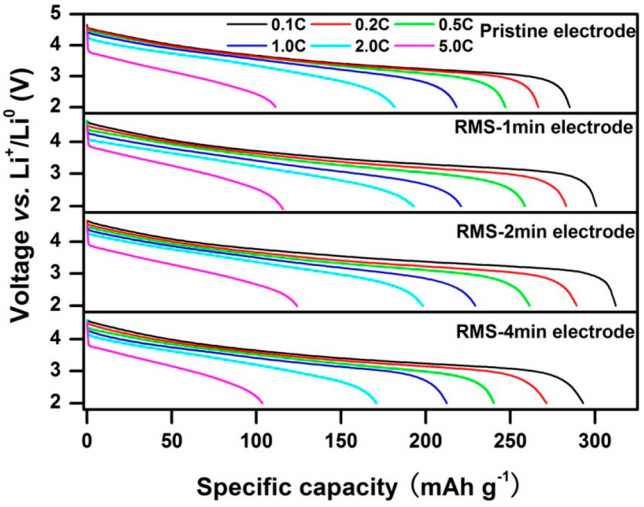

Figure 7. Comparisons of the rate capabilities of different electrodes, where the charge−discharge rates are the same after initial two cycles at 0.1 C-rate.

film with different thickness on the electrodes has been successfully acquired by controlling deposited time.

In order to investigate the deposition of ZnO coating on the surface of LMO-NCM particles, EDS is used to examine the compositions of the TEM image at the center and the edge of the pristine electrode and RMS-4 min coated electrode, respectively, labeled as p1, p2 and p3, p4 in Figure 5a and b. The results shown in the right are that the compositions of the pristine electrode with p1 and p2 has no clear difference, but a clear Zn peak is observed only in p4 but not in p3, which demonstrates ZnO coating on the surface of the particles. The Cu peaks are from the copper grid where the TEM sample was placed. To study the details of RMS coatings grown directly on the electrode, high resolution TEM (HRTEM) is used to examine the pristine and RMS-coated electrode. Parts c and d of Figure 5 present HRTEM images of a bare particle and a RMS-4 min coated particle. It is noted that the particle on the pristine electrode has lattice fringes as observed in Figure 5d, while HRTEM image of the RMS-4 min coated electrode (Figure 5d) reveals that a very thin and amorphous coating fully and conformally enwraps around the crystalline particle. The thickness of the coating is estimated at approximately 8 nm. Therefore, from the XPS and TEM results in Figures 4 and 5, it is concluded that ZnO RMS coatings are ultrathin, dense, uniform, and provide full coverage of LMO-NCM electrode.

3.2. Electrochemical Performances. Figure 6a and b show the first and second charge−discharge profiles of the pristine, RMS-1, 2, and 4 min coated LLNCMO electrodes at a current density of 25 mA g^{-1}. A long plateau around the high potential region (4.4−4.8 V), as shown in Figure 6a, is observed in the first charge profile of all the electrodes, which has been mainly ascribed to the electrochemical activation process of the Li_2MnO_3 component;[12,19] however, this plateau region disappears in the subsequent charge profiles shown in Figure 6b, indicating that the oxygen loss during the first charge is an irreversible process.[21] The initial discharge capacities of the pristine, RMS-1, 2, and 4 min coated electrodes are 283.4 mAh g^{-1}, 300.1 mAh g^{-1}, 316.0 mAh g^{-1}, 293.4 mAh g^{-1}, respectively. In comparison with the capacity between the pristine and RMS coated electrodes, it is clear that the capacity is largely enhanced by the RMS coatings, especially for RMS-2 min coated electrode, of which has significantly exceeded 300 mAh g^{-1}. In addition, the initial coulombic efficiency is acquired to 89.1% for the RMS-2 min coated electrode compared to that of 81.7% for the pristine electrode. Moreover,

dx.doi.org/10.1021/am501293y | ACS Appl. Mater. Interfaces 2014, 6, 9185−9193

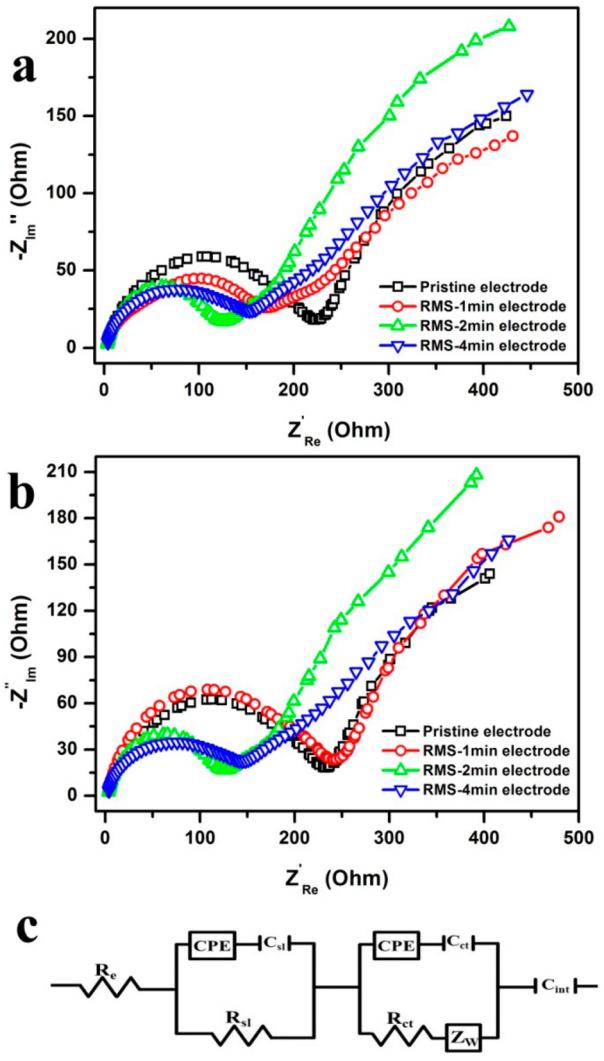

Figure 8. Nyquist plots for different electrodes: (a) after initially charged to 4.5 V, (b) after initially charged to 4.8 V at the current density of 25 mA g^{-1}, and (c) the equivalent circuit performed to fit the curves.

Table 1. Impedance Parameters of the Pristine and RMS-Coated Electrodes after Initially Charged to 4.5 and 4.8 V

	after initially charged to 4.5 V			after initially charged to 4.8 V		
	R_e (Ω)	R_{sl} (Ω)	R_{ct} (Ω)	R_e (Ω)	R_{sl} (Ω)	R_{ct} (Ω)
pristine electrode	2.40	37.2	173.6	3.15	75.1	231.6
RMS-1 min electrode	2.32	106.5	165.7	3.14	167.8	230.4
RMS-2 min electrode	2.24	150.6	105.2	2.42	156.5	116.1
RMS-4 min electrode	1.27	1221	119.8	2.45	1475	154.4

the initial coulombic efficiencies for other two coated electrodes (87.2% and 86.5%) are also larger than that of the pristine electrode. The significant improvement of RMS-coated electrode is possibly ascribed to the uniform and dense ZnO coatings can average the distribution of electrons and lithium ions around the LMO-NCM surface to fully utilize the active sites. This leads to the decrease of the electrode polarizations[53] as presented in Figure 6a and b. It is evident that the first and second charge curve for the RMS-2 min electrode is lower than that of the pristine electrode when the cut-off voltage is below 4.4 V.

The cycle performances of the pristine and RMS-coated electrodes are investigated with a 0.1 and 1.0 C charge–discharge rate (Figure 6c and d). The pristine electrode shows a discharge capacity 238.4 and 157.8 mAh g^{-1} at 0.1 and 1.0C-rate after 50 cycles. Comparatively, the RMS-coated electrodes exhibit relatively higher discharge capacity at 0.1C-rate after 50 cycles. It is noted that the RMS-2 min coated electrode could deliver high discharge capacity of 256.7 mAh g^{-1} at 0.1 C-rate after 50 cycles. However, all the electrodes present a large capacity fading before 15 cycles in Figure 6c, which is possibly associated with the largely structural rearrangement as previously reported.[52] On subsequent cycles, the discharge capacity keeps nearly stable for all electrodes. Additionally, the discharge capacity at 1.0 C-rate for the RMS-2 min coated electrode is about 238 mAh g^{-1}, and the capacity retention is approximately 78.8%, compared with the of 220 mAh g^{-1} and 71.6% for the pristine electrode. It ensures that the ZnO films coatings on the electrode, which effectively protect active material from electrolyte corrosion, can be beneficial to rate capacity and cycle stability during the cycling.

Figure 7 compares the discharge profiles at various C rates of the pristine and RMS-coated electrodes to evaluate their rate capability. The RMS-coated electrodes, especially for RMS-2 min coating, show much higher rate capability than that of the pristine sample. For instance, while the pristine electrode exhibits a discharge capacity of only 181.6 mAh g^{-1} and 112.3 mAh g^{-1} at 2.0 and 5.0 C-rate, the RMS-2 min electrode exhibits 198.3 mAh g^{-1} and 124 mAh g^{-1}, respectively. On the contrary, the RMS-4 min electrode shows higher discharge capacity than that of the pristine electrode at lower rates, however, with the rate increasing to 1.0 C-rate, the discharge capacity is much lower than that of the pristine electrode, which may be ascribed to the coating film increasing to prevent the lithium fast diffusion.

To gain a better understanding of factors leading to the improved electrochemical performance of these coated electrodes, EIS is also introduced to investigate their electrochemical kinetics, which is conducted after initially charged to 4.5 and 4.8 V, and is shown in Figure 8a and b. It can be seen that all the Nyquist plots show two arcs in the high-to-medium frequency region. According to previous EIS studies on this type of layered cathode materials,[26] the first semicircle is contributed to lithium ion diffusion through the surface layer, the second semicircle is assigned to the charge transfer reaction. The corresponding equivalent circuit is given in Figure 8c. In the equivalent circuit, R_e refers to the uncompensated ohmic resistance between the working electrode and the reference electrode, R_{sl} represents the resistance for lithium ion diffusion in the surface layer (including SEI layer and surface modification layer), CPE and C_{sl} refer to the nonideal capacitance of the surface layer and the surface layer capacitance, R_{ct} and C_{ct} refer to the charge transfer resistance and the charge transfer capacitance, Z_w represents the Warburg impedance describing the lithium ion diffusion in the bulk material, and C_{int} presents the intercalation capacitance. Among these parameters, R_e, R_{ct}, and Z_w can be used to quantify the ohmic polarization, charge transfer polarization, and diffusion polarization.[21,22] The fitted impedance parameters are listed in Table 1. It is clear that there is a larger reduction in charge transfer resistance for the RMS-2 min coated electrode than

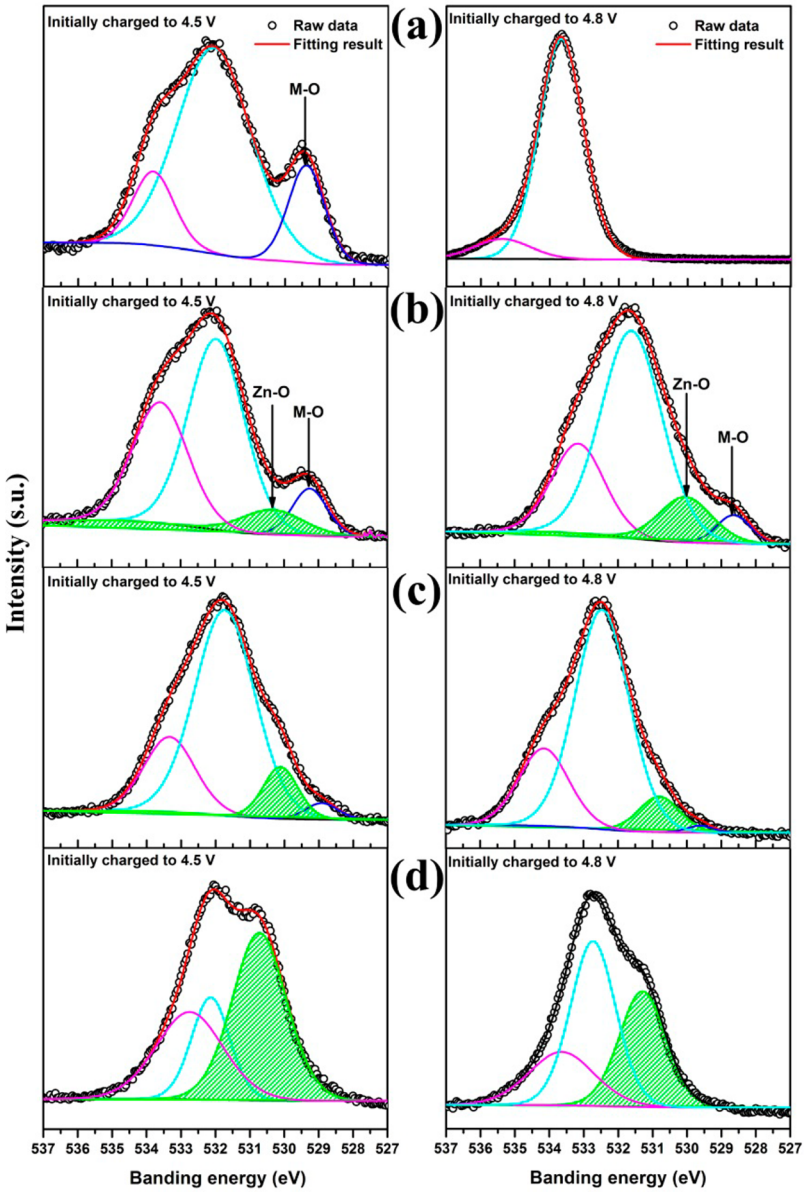

Figure 9. XPS spectra about the O 1s with different electrodes after initially charged to 4.5 and 4.8 V: (a) pristine electrode, (b) RMS-1 min electrode, (c) RMS-2 min electrode, and (d) RMS-4 min electrode.

that of the pristine electrode, whatever the upper charge cut-off voltages are applied to 4.5 and 4.8 V. The resistances for the RMS-coated electrodes have no clear increase for this different charge of sates, while that of the pristine electrode shows the great increase. At the same time, the resistance for lithium ion diffusion for the RMS-4 min coated electrode has a huge increase, which is mainly ascribed to the coating film increasing. This clearly reveals that the charge transfer resistance is greatly reduced in the RMS-2 min coated electrode to improve the electrochemical performance.

Along with EIS study at different state of the charge after initially charged to 4.5 and 4.8 V, XPS of charged electrodes were carried out to determine the chemical composition of passivation products formed as results of high voltage charging. A significant change is expected to occur upon high voltage charging: surface species formation with oxidation of electrolyte. Due to the limitation of the depth of penetration for the XPS, the electrolyte oxidation products layer may screen some signal from surface of lithium-rich layered oxide particle.[48] Figure 9a presents XPS spectra about the O 1s with different electrodes after initially charged to 4.5 and 4.8 V for the pristine electrode. It is observed that there has more obvious electrolyte oxidation when the pristine electrode is initially charged to 4.8 V than that initially charged to 4.5 V. This results in the disappearance of the lattice oxygen 1s signal in lithium-rich layered oxides. Instead, some electrolyte oxidation products exist in the particle surface and leads to the resistance increasing as given in Table 1 demonstrated by EIS measurements. By contrast, the O 1s signals for RMS-coated electrodes have no clear change as shown in Figure 9b–d, even if the initial charge voltage gets to 4.8 V. The less the electrolyte oxidation occurs, the lower the resistance, and the better the electrochemical performance. On the other hand, the O 1s spectra for the RMS-coated electrodes after initially charged 4.5 or 4.8 V show the similar results with the uncharged RMS-coated electrode. The slight difference is that the higher binding energy is shifted to

dx.doi.org/10.1021/am501293y | ACS Appl. Mater. Interfaces 2014, 6, 9185–9193

larger value, which is usually attributed to C−O compounds that may be originated from the electrolyte oxidation.[48] Additionally, when the RMS-2 min electrode is initially charged to 4.8 V, the O 1s signal in the ZnO films on the surface, and more importantly, the lattice oxygen signal in lithium-rich layered oxides are still clearly observed in Figure 9b and c. This further indicates that the existence of ZnO coatings on the electrode surface could prevent the electrolyte oxidation to a certain degree. On the basis of these results, it is concluded that ZnO surface coatings on the electrodes by RMS process play an important role in improving the electrochemical performance, due to the suppression of the electrolyte oxidation to decrease the resistance, especially for the charge transfer resistance. As a consequence, the decrease of the charge transfer resistance could greatly improve the rate capability and the protective layer of ZnO film on the electrode surface could enhance the electrode surface stability to improve the cycling performance.

4. CONCLUSION

We have successfully fabricated LMO-NCM electrode films modified by RMS ZnO coatings for the first time. Presence of ZnO coatings on the electrode was confirmed by XPS and TEM study. The coatings were ultrathin, dense, uniform, and provided full coverage of LMO-NCM electrode surface. It has been realized from our experimental studies that the RMS-2 min ZnO coated on the LMO-NCM electrodes had the following superiorities compared to pristine LMO-NCM: (i) ultrahigh discharge capacity of 316.0 mAh g^{-1} at room temperature; (ii) higher initial columbic efficiency with 89.1% than that of 81.7%; (iii) improved rate performance with discharge capacity of 238.0 mAh g^{-1} at 1.0 C-rate for the RMS-2 min coated electrode. Lower charge transfer resistance value in case of the RMS-coated electrode enhanced the electrochemical performance compared to pristine sample. ZnO surface coatings on the electrodes by RMS process play an important role in suppression of the electrolyte oxidation to improve the cycling performance. Lastly, the method presented in this study can be generalized to other coatings as long as the coatings can be fabricated via RMS, which could be directly deposited from single or multiple metallic targets.

AUTHOR INFORMATION

Corresponding Authors

*Tel.: +86 574 86685096. Fax: +86 574 86685096. Email: xiayg@nimte.ac.cn.
*Email: liuzp@nimte.ac.cn.

Notes

The authors declare no competing financial interest.

ACKNOWLEDGMENTS

We are grateful for financial support from the Key Research Program of Chinese Academy of Sciences (Grant No. KGZD-EW-202-4), Ningbo Science and Technology Innovation Team (Grant No. 2012B82001), and the 973 program (Grant No. 2011CB935900). The authors acknowledge Dr. Ruijin Hong for preparing the coating films on the electrodes by reactive magnetron sputtering.

REFERENCES

(1) Armand, M.; Tarascon, J. M. Building Better Batteries. *Nature* **2008**, *451*, 652−657.
(2) Arico, A. S.; Bruce, P.; Scrosati, B.; Tarascon, J. M.; Schalkwijk, W. V. Nanostructured Materials for Advanced Energy Conversion and Storage Devices. *Nat. Mater.* **2005**, *4*, 366−377.
(3) Thackeray, M. M.; Wolverton, C.; Isaacs, E. D. Electrical Energy Storage for Transportation-Approaching the Limits of, and Going Beyond, Lithium-Ion Batteries. *Energy Environ. Sci.* **2012**, *5*, 7854−7863.
(4) He, P.; Yu, H. J.; Li, D.; Zhou, H. S. Layered Lithium Transition Metal Oxide Cathodes towards High Energy Lithium-Ion Batteries. *J. Mater. Chem.* **2012**, *22*, 3680−3695.
(5) Ellis, B. L.; Lee, K. T.; Nazar, L. F. Positive Electrode Materials for Li-Ion and Li-Batteries. *Chem. Mater.* **2010**, *22*, 691−714.
(6) Xu, B.; Qian, D. N.; Wang, Z. Y.; Meng, Y. S. Recent Progress in Cathode Materials Research for Advanced Lithium Ion Batteries. *Mater. Sci. Eng. R* **2012**, *73*, 51−65.
(7) Lu, Z. H.; MacNeil, D. D.; Dahn, J. R. Layered Cathode Materials $Li[Ni_xLi_{(1-2x/3)}Mn_{(2/3-x/3)}]$ O_2 for Lithium-Ion Batteries. *Electrochem. Solid-State Lett.* **2001**, *4*, A191−A194.
(8) Thackeray, M. M.; Kang, S.-H.; Johnson, C. S.; Vaughey, J. T.; Benedek, R.; Hackney, S. A. Li_2MnO_3-Stabilized $LiMO_2$ (M = Mn, Ni, Co) Electrodes for Lithium-Ion Batteries. *J. Mater. Chem.* **2007**, *17*, 3112−3125.
(9) Ohzuku, T.; Nagayama, M.; Tsuji, K.; Ariyoshi, K. High-Capacity Lithium Insertion Materials of Lithium Nickel Manganese Oxides for Advanced Lithium-Ion Batteries: Toward Rechargeable Capacity more than 300 mA h g^{-1}. *J. Mater. Chem.* **2011**, *21*, 10179−10188.
(10) Yabuuchi, N.; Yoshii, K.; Myung, S.-T.; Nakai, I.; Komaba, S. Detailed Studies of a High-Capacity Electrode Material for Rechargeable Batteries, Li_2MnO_3−$LiCo_{1/3}Ni_{1/3}Mn_{1/3}O_2$. *J. Am. Chem. Soc.* **2011**, *133*, 4404−4419.
(11) Yu, H. J.; Zhou, H. S. High-Energy Cathode Materials (Li_2MnO_3−$LiMO_2$) for Lithium-Ion Batteries. *J. Phys. Chem. Lett.* **2013**, *4*, 1268−1280.
(12) Yu, H. J.; Kim, H. J.; Wang, Y. R.; He, P.; Asakura, D.; Nakamura, Y.; Zhou, H. S. High-Energy 'Composite' Layered Manganese-Rich Cathode Materials via Controlling Li_2MnO_3 Phase Activation for Lithium-Ion Batteries. *Phys. Chem. Chem. Phys.* **2012**, *14*, 6584−6595.
(13) Qiu, B.; Wang, J.; Xia, Y. G.; Liu, Y. Z.; Qin, L. F.; Yao, X. Y.; Liu, Z. P. Effects of Na^+ Contents on Electrochemical Properties of $Li_{1.2}Ni_{0.13}Co_{0.13}Mn_{0.54}O_2$ Cathode Materials. *J. Power Sources* **2013**, *240*, 530−535.
(14) Wang, J.; Qiu, B.; Cao, H. L.; Xia, Y. G.; Liu, Z. P. Electrochemical Properties of $0.6Li[Li_{1/3}Mn_{2/3}]O_2$−$0.4LiNi_xMn_yCo_{1-x-y}O_2$ Cathode Materials for Lithium-Ion Batteries. *J. Power Sources* **2012**, *218*, 128−133.
(15) Qiu, S.; Chen, Z. X.; Pei, F.; Wu, F. Y.; Wu, Y.; Ai, X. P.; Yang, H. X.; Cao, Y. L. Synthesis of Monoclinic $Li[Li_{0.2}Ni_{0.13}Co_{0.13}Mn_{0.54}]O_2$ Nanoparticles by a Layered-Template Route for High-Performance Li-Ion Batteries. *Eur. J. Inorg. Chem.* **2013**, *2013*, 2887−2892.
(16) Zhao, C. H.; Wang, X. X.; Liu, X. R.; Zhang, H.; Shen, Q. Mn−Ni Content-Dependent Structures and Electrochemical Behaviors of Serial $Li_{1.2}Ni_{0.13+x}Co_{0.13}Mn_{0.54-x}O_2$ as Lithium-Ion battery Cathodes. *ACS Appl. Mater. Interfaces* **2014**, *6*, 2386−2392.
(17) Jiang, K.-C.; Wu, X.-L.; Yin, Y.-X.; Lee, J.-S.; Kim, J.; Guo, Y.-G. Superior Hybrid Cathode Material Containing Lithium-Excess Layered Material and Graphene for Lithium-Ion Batteries. *ACS Appl. Mater. Interfaces* **2012**, *4*, 4858−4863.
(18) Yu, H. J.; Wang, Y. R.; Asakura, D.; Hosono, E.; Zhang, T.; Zhou, H. S. Electrochemical Kinetics of the $0.5Li_2MnO_3$−$0.5LiMn_{0.42}Ni_{0.42}Co_{0.16}O_2$ 'Composite' Layered Cathode Material for Lithium-Ion Batteries. *RSC Adv.* **2012**, *2*, 8797−8807.
(19) Armstrong, A. R.; Holzapfel, M.; Novák, P.; Johnson, C. S.; Kang, S.-H.; Thackeray, M. M.; Bruce, P. G. Demonstrating Oxygen Loss and Associated Structural Reorganization in the Lithium Battery Cathode $Li[Ni_{0.2}Li_{0.2}Mn_{0.6}]O_2$. *J. Am. Chem. Soc.* **2006**, *128*, 8694−8698.
(20) Xu, B.; Fell, C. R.; Chi, M. F.; Meng, Y. S. Identifying Surface Structural Changes in Layered Li-excess Nickel Manganese Oxides in

High Voltage Lithium Ion Batteries: A Joint Experimental and Theoretical Study. *Energy Environ. Sci.* **2011**, *4*, 2223−2233.
(21) Wang, Q. Y.; Liu, J.; Murugan, A. V.; Manthiram, A. High Capacity Double-layer Surface Modified $Li[Li_{0.2}Ni_{0.13}Co_{0.13}Mn_{0.54}]O_2$ Cathode with Improved Rate Capability. *J. Mater. Chem.* **2009**, *19*, 4965−4972.
(22) Guo, S. H.; Yu, H. J.; Liu, P.; Liu, X. Z.; Li, D.; Chen, M. W.; Ishida, M.; Zhou, H. S. Surface Coating of Lithium-Manganese-Rich Layered Oxides with Delaminated MnO_2 Nanosheets as Cathode Materials for Li-Ion Batteries. *J. Mater. Chem. A* **2014**, *2*, 4422−4428.
(23) Wu, F.; Wang, Z.; Su, Y. F.; Yan, N.; Bao, L. Y.; Chen, S. $Li[Li_{0.2}Ni_{0.13}Co_{0.13}Mn_{0.54}]O_2$-$MoO_3$ Composite Cathodes with Low Irreversible Capacity Loss for Lithium Ion Batteries. *J. Power Sources* **2014**, *247*, 20−25.
(24) Min, J. W.; Yim, C. J.; Im, W. B. Facile Synthesis of Electrospun $Li_{1.2}Ni_{0.17}Co_{0.17}Mn_{0.5}O_2$ Nanofiber and Its Enhanced High-Rate Performance for Lithium-Ion Battery Applications. *ACS Appl. Mater. Interfaces* **2013**, *5*, 7765−7769.
(25) Wang, J.; He, X.; Kloepsch, R.; Wang, S. H.; Hoffmann, B.; Jeong, S.; Yang, Y.; Li, J. Increased Capacity of $LiNi_{1/3}Co_{1/3}Mn_{1/3}O_2$-$Li[Li_{1/3}Mn_{2/3}]O_2$ Cathodes by MnO_x-Surface Modification for Lithium-Ion Batteries. *Energy Technol.* **2014**, *2*, 188−193.
(26) Zheng, J. M.; Zhang, Z. R.; Wu, X. B.; Dong, Z. X.; Zhu, Z.; Yang, Y. The Effects of AlF_3 Coating on the Performance of $Li[Li_{0.2}Ni_{0.13}Co_{0.13}Mn_{0.54}]O_2$ Positive Electrode Material for Lithium-Ion Battery. *J. Electrochem. Soc.* **2008**, *155*, A775−A782.
(27) Kang, S.-H.; Thackeray, M. M. Enhancing the Rate Capability of High Capacity xLi_2MnO_3−$(1-x)LiMO_2$ (M = Mn, Ni, Co) Electrodes by Li−Ni−PO_4 Treatment. *Electrochem. Commun.* **2009**, *11*, 748−751.
(28) Jung, Y. S.; Cavanagh, A. S.; Yan, Y. F.; George, S. M.; Manthiram, A. Effects of Atomic Layer Deposition of Al_2O_3 on the $Li[Li_{0.2}Ni_{0.13}Co_{0.13}Mn_{0.54}]O_2$ Cathode for Lithium-Ion Batteries. *J. Electrochem. Soc.* **2011**, *158*, A1298−A1302.
(29) Scott, I. D.; Jung, Y. S.; Cavanagh, A. S.; Yan, Y. F.; Dillon, A. C.; George, S. M.; Lee, S.-H. Ultrathin Coatings on Nano-$LiCoO_2$ for Li-Ion Vehicular Applications. *Nano Lett.* **2011**, *11*, 414−418.
(30) Zhao, J. Q.; Wang, Y. Ultrathin Surface Coatings for Improved Electrochemical Performance of Lithium Ion Battery Electrodes at Elevated Temperature. *J. Phys. Chem. C* **2012**, *116*, 11867−11876.
(31) Liu, J.; Jayan, B. R.; Manthiram, A. Conductive Surface Modification with Aluminum of High Capacity Layered $Li[Li_{0.2}Ni_{0.13}Co_{0.13}Mn_{0.54}]O_2$ Cathodes. *J. Phys. Chem. C* **2010**, *114*, 9528−9533.
(32) Liu, J.; Wang, Q. Y.; Jayan, B. R.; Manthiram, A. Carbon-Coated High Capacity Layered $Li[Li_{0.2}Ni_{0.13}Co_{0.13}Mn_{0.54}]O_2$ Cathodes. *Electrochem. Commun.* **2010**, *12*, 750−753.
(33) Shin, D. W.; Choi, J.-W.; Ahn, J.-P.; Choi, W.-K.; Cho, Y. S.; Yoon, S.-J. ZrO_2-Modified $LiMn_2O_4$ Thin-Film Cathodes Prepared by Pulsed Laser Deposition. *J. Electrochem. Soc.* **2010**, *157*, A567−A570.
(34) Hong, R. J.; Qi, H. J.; Huang, J. B.; He, H. B.; Fan, Z. X.; Shao, J. D. Influence of Oxygen Partial Pressure on the Structure and Photoluminescence of Direct Current Reactive Magnetron Sputtering ZnO Thin Films. *Thin Solid Films* **2005**, *473*, 58−62.
(35) Li, L.; Fang, L.; Zhou, X. J.; Liu, Z. Y.; Zhao, L.; Jiang, S. X-ray Photoelectron Spectroscopy Study and Thermoelectric Properties of Al-Doped ZnO Thin Films. *J. Electron. Spectrosc. Relat. Phenom.* **2009**, *173*, 7−11.
(36) Ellmer, K. Magnetron Sputtering of Transparent Conductive Zinc Oxide: Relation Between the Sputtering Parameters and the Electronic Properties. *J. Phys., D: Appl. Phys.* **2000**, *33*, R17.
(37) Lee, K.-L.; Jung, J.-Y.; Lee, S.-W.; Moon, H.-S.; Park, J.-W. Electrochemical Characteristics and Cycle Performance of $LiMn_2O_4$/*a*-Si Microbattery. *J. Power Sources* **2004**, *130*, 241−246.
(38) Fischer, J.; Adelhelm, C.; Bergfeldt, T.; Chang, K.; Ziebert, C.; Leiste, H.; Stüber, M.; Ulrich, S.; Music, D.; Hallstedt, B.; Seifert, H. J. Development of Thin Film Cathodes for Lithium-Ion Batteries in the Material System Li-Mn-O by r.f. Magnetron Sputtering. *Thin Solid Films* **2013**, *528*, 217−223.
(39) Wu, Y.; Manthiram, A. Effect of Surface Modifications on the Layered Solid Solution Cathodes $(1-z)Li[Li_{1/3}Mn_{2/3}]O-(z)$ $Li[Mn_{0.5-y}Ni_{0.5-y}Co_{2y}]O_2$. *Solid State Ionics* **2009**, *180*, 50−56.
(40) Singh, G.; Thomas, R.; Kumar, A.; Katiyar, R. S.; Manivannan, A. Electrochemical and Structural Investigations on ZnO Treated $0.5Li_2MnO_3$−$0.5LiMn_{0.5}Ni_{0.5}O_2$ Layered Composite Cathode Material for Lithium-Ion Battery. *J. Electrochem. Soc.* **2012**, *159*, A470−A 478.
(41) Wang, J.; Yuan, G. X.; Zhang, M. H.; Qiu, B.; Xia, Y. G.; Liu, Z. P. The Structure, Morphology, and Electrochemical Properties of $Li_{1+x}Ni_{1/6}Co_{1/6}Mn_{4/6}O_{2.25+x/2}$ $(0.1 \leq x \leq 0.7)$ Cathode Materials. *Electrochim. Acta* **2012**, *66*, 61−66.
(42) Yu, H. J.; Ishikawa, R.; So, Y.-G.; Shibata, N.; Kudo, T.; Zhou, H. S.; Ikuhara, Y. Direct Atomic-Resolution Observation of Two Phases in the $Li_{1.2}Mn_{0.567}Ni_{0.166}Co_{0.067}O_2$ Cathode Material for Lithium-Ion Batteries. *Angew. Chem. Int. Ed.* **2013**, *52*, 5969−5973.
(43) Blumentrit, P.; Yoshitakea, M.; Neḿsáka, S.; Kima, T.; Nagata, T. XPS and UPS Study on Band Alignment at Pt-Zn-Terminated ZnO (0001) Interface. *Appl. Surf. Sci.* **2011**, *258*, 780−785.
(44) Guo, R.; Shi, P. F.; Cheng, X. Q.; Sun, L. Effect of ZnO Modification on the Performance of $LiNi_{0.5}Co_{0.25}Mn_{0.25}O_2$ Cathode Material. *Electrochim. Acta* **2009**, *54*, 5796−5803.
(45) Baggetto, L.; Dudney, N. J.; Veith, G. M. Surface Chemistry of Metal Oxide Coated Lithium Manganese Nickel Oxide Thin Film Cathodes Studied by XPS. *Electrochim. Acta* **2013**, *90*, 135−147.
(46) Fell, C. R.; Carroll, K. J.; Chi, M. F.; Meng, Y. S. Synthesis-Structure−Property Relations in Layered, "Li-Excess" Oxides Electrode Materials $Li[Li_{1/3-2x/3}Ni_xMn_{2/3-x/3}]O_2$ (x = 1/3, 1/4, and 1/5). *J. Electrochem. Soc.* **2010**, *157*, A1202−A1211.
(47) Hsieh, P.-T.; Chen, Y.-.C.; Kao, K.-S.; Wang, C.-M. Luminescence Mechanism of ZnO Thin Film Investigated by XPS Measurement. *Appl. Phys. A* **2008**, *90*, 317−321.
(48) Martha, S. K.; Nanda, J.; Veith, G. M.; Dudney, N. J. Surface Studies of High Voltage Lithium Rich Composition: $Li_{1.2}Mn_{0.525}Ni_{0.175}Co_{0.1}O_2$. *J. Power Sources* **2012**, *216*, 179−186.
(49) Chen, M.; Wang, X.; Yu, Y. H.; Pei, Z. L.; Bai, X. D.; Sun, C.; Huang, R. F.; Wen, L. S. X-ray Photoelectron Spectroscopy and Auger Electron Spectroscopy Studies of Al-Doped ZnO Films. *Appl. Surf. Sci.* **2000**, *158*, 134−140.
(50) Kunat, M.; Girol, S. G.; Burghaus, U.; Wo1ll, C. The Interaction of Water with the Oxygen-Terminated, Polar Surface of ZnO. *J. Phys. Chem. B* **2003**, *107*, 14350−14356.
(51) Kotsis, K.; Staemmler, V. *Ab Initio* Calculations of the O1s XPS Spectra of ZnO and Zn oxo Compounds. *Phys. Chem. Chem. Phys.* **2006**, *8*, 1490−1498.
(52) Jiang, M.; Key, B.; Meng, Y. S.; Grey, C. P. Electrochemical and Structural Study of the Layered, "Li-Excess" Lithium-Ion Battery Electrode Material $Li[Li_{1/9}Ni_{1/3}Mn_{5/9}]O_2$. *Chem. Mater.* **2009**, *21*, 2733−2745.
(53) Yu, H. J.; Zhou, H. S. Initial Coulombic Efficiency Improvement of the $Li_{1.2}Mn_{0.567}Ni_{0.166}Co_{0.067}O_2$ Lithium-Rich Material by Ruthenium Substitution for Manganese. *J. Mater. Chem.* **2012**, *22*, 15507−15510.